



Keywords

WT Shapes,
Eccentrically Loaded,
Eccentric Loading,
Compression,
Design Tables

Received: July 25, 2017

Accepted: August 14, 2017

Published: September 20, 2017

A Closer Examination of Design Approaches for Eccentrically Loaded WT Shapes in Compression

Yuwen Li

Gannett Fleming Inc., Valley Forge, Pennsylvania, United States

Email address

yli@gfnet.com

Citation

Yuwen Li. A Closer Examination of Design Approaches for Eccentrically Loaded WT Shapes in Compression. *American Journal of Civil and Environmental Engineering*. Vol. 2, No. 5, 2017, pp. 37-56.

Abstract

Design strengths of Structural Tees (WT-shapes, Tees) in axial compression are provided in Table 4-5 of the 14th edition of *AISC Manual of Steel Construction (the Manual)* [1], with an assumption that the compression force is applied at the center of gravity (c.g.) of the cross section. However, in engineering practice, Tees are rarely loaded at the section's c.g.; rather, they are eccentrically loaded at the ends through the gusset plates that welded or bolted to their flanges. Therefore, these Tees are subject to the axial compressive force and the bending moment induced by the eccentric end connections. Although the design strengths of eccentrically loaded WT-shapes are not provided in *the Manual*, they can be calculated based on *AISC Specifications for Structural Steel Constructions (the Specifications)* [2], albeit the design process is tedious and time consuming. However, if *the Specifications* are indiscriminately followed (called Approach 1 in this paper), the calculated strengths are too conservative. This paper discusses an alternate approach (Approach 2) allowed for by Commentary H2 of *the Specifications*, and the calculated strengths based on Approach 2 are larger and more reasonable than those based on Approach 1. Extensive Finite Element Nonlinear Analyses have been employed to validate the proposed approach. Finally, design tables for eccentrically loaded WT-shapes are provided to help engineers quickly determine the proper size of a WT-shape for their project.

1. Introduction

WT-shapes are commonly used in the bracing system to resist large axial loads and/or to satisfy the KL/r requirement for large unbraced lengths. When used as braces, Tees are often connected to a gusset plate through their flanges which create an eccentric connection due to an offset between the neutral axis of the Tee and the gusset plate. Although braces are treated as truss members in the structural analysis, the induced bending moment on a Tee due to the eccentric connection must be considered in the member design. This additional bending moment is neither considered by design tables in the 14th edition of *AISC Manual of Steel Construction* [1], nor by *Design Examples, Version 14* [3].

Gordon [4] presented *Tables for Eccentrically Loaded WT Shapes in Compression*, based on the 13th edition of *AISC Manual of Steel Construction (AISC 2005)*, but it is the author's opinion that while the available strengths from Gordon's tables are conservative (called Approach 1 in this paper), more capacity is available if a different design approach is used. This paper discusses an alternative approach (Approach 2) permitted by *the Specifications* [2] that yields larger and much needed capacities.

2. Observation

Although the predominant load in Tee bracing and cross-frame members is the axial load, the effect of bending moments must be accounted for in the member design. Two components contribute to the moment in a Tee used as a brace: one is the moment due to the selfweight; the other is the moment due to an eccentric end connection. The moment due to selfweight can be neglected for bracing members with short lengths; however this moment should be considered in the design of long, slender bracing members. The effect of selfweight is not discussed in this paper.

To demonstrate the conservativeness of Approach 1, consider two 10 ft. long grade 36 steel brace members: one uses WT6×17.5 with flange connected to a 5/8-in. thick gusset plate; another uses a single angle L6×6×7/16 with one leg

connected to a 5/8-in. thick gusset plate (*Figure 1*). The available axial compressive strength of the Tee member is based on Design Approach 1 (see Example in later section); the available axial compressive strength of single angle member is from *Table 4-12 of the Manual* [1], or can be easily computed based on Section E5 of *the Specifications* [2], as discussed by Li [10]. The results are presented in *Table 1*.

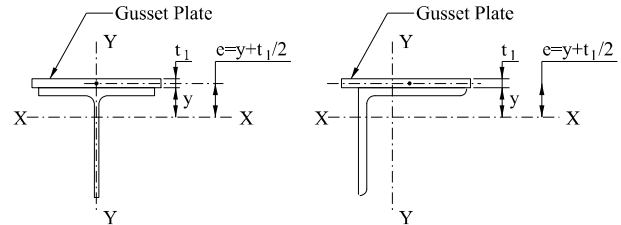


Figure 1. Tee & Single Angle Braces.

Table 1. Comparison of the Available Compressive Strength of WT6×17.5 & L6×6×7/16.

Section	Wt. (lb/ft)	Connected element	Outstanding Element	$\phi_c P_n$ (kips)	Reference
WT6×17.5	17.5	6.56×0.52	5.48×0.30	48.8	Example
L6×6×7/16	17.3	6.00×0.44	5.56×0.44	76.2	Sec. E5 of <i>the Specifications</i>
				62.4	Table 4-12 of <i>the Manual</i>

In terms of member weight, element size and thickness, the single angle L6×6×7/16 is very close to WT6×17.5. Intuitively WT6×17.5 should have a larger axial capacity than the single angle L6×6×7/16 since it is a singly symmetric section and the bending is in the plane of symmetry. However, the axial capacity of the Tee based on Design Approach 1 is only about 64% of that of the single angle; therefore, the available strengths of eccentrically loaded Tees deserve a closer examination.

To further illustrate the significance of the low capacities based on Design Approach 1, both the Tee and single angle are investigated for a range of unbraced length from 4 ft. to 19 ft., and the results are shown in *Figure 2*.

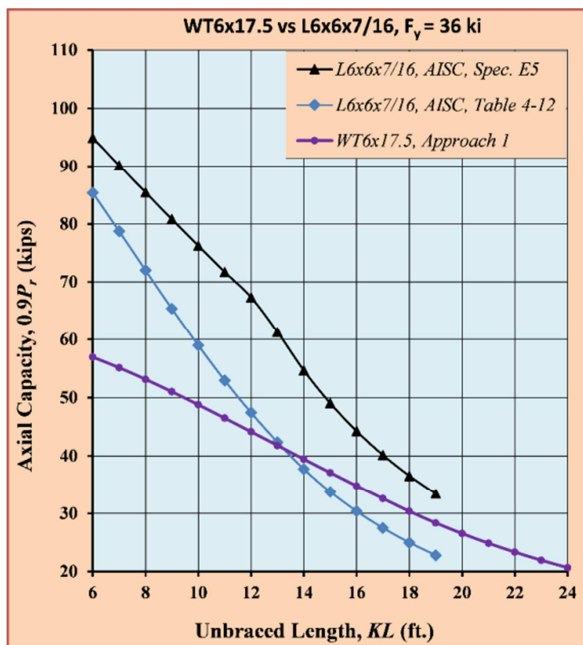


Figure 2. Axial Capacities of Tee and Single Angle.

3. Behavior of WT Shapes

In applications such as bracings and cross-frames, the Tee can be connected to a gusset plate through either the flange or the stem. Connection through the stem (*Figure 3*) is rarely used for the practical reasons. In order to connect a gusset plate to the stem, half of the flange must be coped to accept the gusset plate, which adds to the fabrication cost. However, a gusset attached to the stem minimizes the eccentricity from the neutral axis of the Tee; Tees connected in this manner can be designed as concentrically loaded members if the selfweight induced moment is negligible in design, and Table 4-7 of *the Manual* [1] can be used to obtain its available axial compressive capacities.

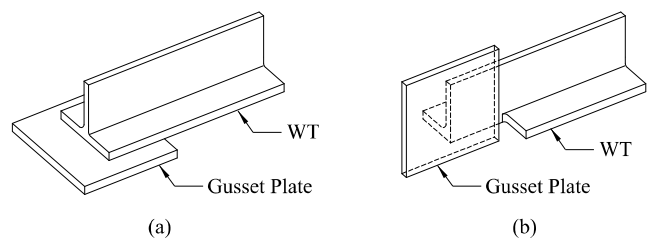


Figure 3. End Connection Types of WT-Members.

Tees are singly symmetric sections about the centerline of the stem. A connection through the flange (*Figure 3*) is a commonly used engineering practice due to the simplicity of the connection; however, this type of connection creates an eccentricity from the neutral axis of the Tee from the applied load. The effect of connection eccentricity is a function of connection and member stiffness, if the connection is through a thin gusset plate, the moment due to connection eccentricity cannot be resisted by the thin plate at the connection; the moment must be resisted by the member [2] (*Figure 4*). This moment will reduce the axial capacity of the member.

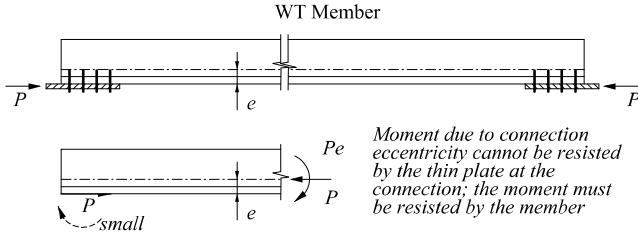


Figure 4. Connection Moment.

A pure bending moment in the plane of symmetry of a Tee produces bending stress in the tip of the stem that is much greater than the stress in the flange, therefore, the flexural strength of the Tee is controlled by the stress in the stem. However, for a Tee in compression that is eccentrically loaded from its the flange, the magnitude of the induced bending moment is directly proportional to the applied axial load. While the induced moment produces a large tensile stress in the tip of stem, the uniformly distributed compressive stress due to the applied axial load reduces the tensile stress in the stem and increases the compressive stress in the flange caused by the bending moment (Figure 5).

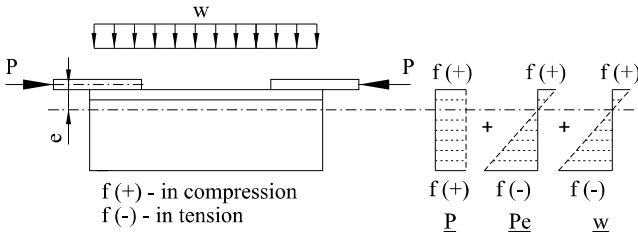


Figure 5. Stresses in WT-Sections.

Compared to the flexural strength of a Tee member in pure bending, the flexural strength of the Tee is increased due to the presence of axial force. Consider a zero length WT6×17.5 member ($A_g = 5.17 \text{ in}^2$, $I_x = 16.0 \text{ in}^4$, $S_x = 3.23 \text{ in}^3$, $d = 6.25 \text{ in}$, and $y = 1.30 \text{ in}$), the pure bending yield capacity $M_y = F_y(S_x) = (36 \text{ ksi})(3.23 \text{ in}^3) = 116.28 \text{ kip-in}$. When the moment is created through an eccentrically loaded axial compressive force, the maximum compressive force and the corresponding moment can be found by solving equations (1) and (2); and the results are $P_r = 108.77 \text{ kips}$, $e = 1.694 \text{ in}$, and $M_y = P_r e = 184.25 \text{ kip-in}$, which is greater than 116.28 kip-in. In other words, when disregarding local and lateral torsional buckling, or when they are not in control, the presence of axial compressive force will increase the flexural capacity when the stem is in tension.

$$\frac{P_r}{A_g} + \frac{P_r e}{I_x} y = \frac{P_r}{5.17} + \frac{P_r e}{16} 1.3 = 36 \quad \text{at tee flange, and} \quad (1)$$

$$\frac{P_r}{A_g} - \frac{P_r e}{S_x} = \frac{P_r}{5.17} - \frac{P_r e}{3.23} = -36 \quad \text{at tee stem} \quad (2)$$

4. Design Approaches

For a Tee with gusset plate connected to its flange, or when the selfweight moment is too significant to be neglected, the

available capacity of the Tee should be determined by considering the interaction of combined forces according to Chapter H of the *Specifications* [2].

Although Tees are singly symmetric sections, no single WT-shape satisfies the $0.1 \leq I_{yc}/I_y \leq 0.9$ requirement of Section H1.1 of the *Specifications* [2]. Therefore, Section H2 should be used to evaluate the capacity of a Tee under combined forces, and Equation H2-1 can be rewritten as:

$$\left| \frac{f_{ra}}{F_{ca}} + \frac{f_{rbx}}{F_{cbx}} + \frac{f_{rby}}{F_{cby}} \right| \leq 1.0 \quad \text{at tee flange, and} \quad (3)$$

$$\left| \frac{f_{ra}}{F_{ca}} - \frac{f_{rbx}}{F_{cbx}} \right| \leq 1.0 \quad \text{at tee stem} \quad (4)$$

where, f_{ra} = required axial stress

F_{ca} = available axial stress

f_{rbx}, f_{rby} = required flexural stress at P.O.C.

F_{cbx}, F_{cby} = available flexural stress at P.O.C.

f_{ra}, f_{rbx} and f_{rby} at the P.O.C. (point of consideration) can be easily obtained using proper section properties and applied forces; F_{ca} can be calculated based on Sections E3 or E4, and F_{cby} can be calculated based on Section F6 of the *Specifications* [2]. However, the computation of F_{cbx} needs a closer examination since the flexural stresses in the flange and in the stem due to the bending about the x-axis involves two distinguished section modulus: S_x and S_{xc} .

As discussed in Commentary H2 of the *Specifications* [2], there are two approaches for using Equation H2-1:

(a) "Strictly using Equation H2-1 for the interaction of the critical moment about each principal axis, there is only one flexural stress ratio term for every critical location since the moment and stress ratios are the same.... The yielding moment should be based on the smallest section modulus about the axis being considered." For a Tee connected through the flange that is in compression, additional compressive stress is introduced in flange due to the eccentricity, the compression in the flange will always control the design since the yield moment is based on the smallest section modulus about x-axis. Therefore, the stress ratio need only be checked for compression at the flange, this approach is called Design Approach 1 in this article.

(b) "For certain load combinations, where the critical stress can transition from tension at one point on the cross section to compression at another, it may be advantageous to consider two interaction relationships depending on the magnitude of each component." For a Tee connected through the flange that is in compression, the introduction of tensile stress due to eccentricity will reduce the compressive stress in stem, it could benefit from consideration of more than one interaction relationship occurs, and the yield moments could be based on section modulus of flange and tip of stem individually. Therefore, the stress ratio need be checked for both stem and flange, although for eccentrically load Tee, the moment induced by eccentricity is small, stress ratio at flange will most likely controls the design, this approach is called

Design Approach 2 in this article.

4.1. Available Flexural Stresses F_{cbx} - Design Approach 1

According to Section E9 of *the Specifications* [2], for Tees loaded in the plane of symmetry, the nominal flexural strength M_{nx} shall be the lowest value obtained according to the *limit states of yielding, lateral torsional buckling, and flange local buckling*, and the available flexural stress F_{cbx} can be calculated as follows:

$$F_{cbx_stem} = \frac{\phi_b M_{nx}}{S_x} \quad (5)$$

$$F_{cbx_flange} = \frac{\phi_b M_{nx}}{S_{xc}} \quad (6)$$

where, S_x , section modulus of the stem, $S_x = I_y / (d - y)$

Table 2. WT with non-compact Flanges ($F_y = 50$ ksi) ($\lambda_{rf} = 24.1 < \lambda < \lambda_{pf} = 9.15$).

Section	$\lambda = b_f / 2t_f$	Section	$\lambda = b_f / 2t_f$	Section	$\lambda = b_f / 2t_f$
WT3x4.5	10.1	WT4x15.5	9.19	WT7x49.5	9.34
WT3x6	9.16	WT5x6	9.43	WT10.5x24	9.47
WT3x7.5	11.5	WT6x32.5	9.92		
WT4x5	9.61	WT7x45	10.2		

The nominal flexural strength of the Tee member, M_{nx} , under the *limit state of yielding* can be calculated as:

$$M_{nx} = M_p = F_y Z_x \leq 1.6 M_{yx} \quad (7)$$

where, Z_x – plastic section modulus

$$M_{yx} = F_y S_x$$

After examining all 273 WT-shapes, it is concluded that the section modulus ratio Z_x / S_x is in the range of 1.75 (WT6x13) to 2.23 (WT7x275), and the nominal yield strength of a Tee is thus controlled by $1.6 F_y S_x$. Therefore the available flexural stress in stem, F_{cbx_stem} and the available flexural stress in flange, F_{cbx_flange} , are:

$$F_{cbx_stem} = \frac{\phi_b M_{nx}}{S_x} = \frac{\phi_b \min(F_y Z_x, 1.6 F_y S_x)}{S_x} = \phi_b (1.6 F_y) \quad (8)$$

$$F_{cbx_flange} = \frac{\phi_b M_{nx}}{S_{xc}} = \frac{\phi_b \min(F_y Z_x, 1.6 F_y S_x)}{S_{xc}} = \frac{\phi_b (1.6 F_y S_x)}{S_{xc}} \quad (9)$$

It is also concluded from AISC Shapes Database v14.0 that the ratio of elastic section modulus of the flange to the elastic section modulus of the stem $S_{xc} / S_x = (d - y) / y$ is in the range of 2.23 (WT7x365) to 5.43 (WT7x45), and thus

S_{xc} , section modulus of the flange $S_{xc} = I_y / y$

The nominal flexural strength of the Tee, M_{nx} , under the *limit state of lateral torsional buckling* should be calculated according to Equation 9-4 of *the Specifications* [2].

The nominal flexural strength of the Tee member, M_{nx} , under the *limit state of flange local buckling* in flexural compression should be determined according to Section F9.3 of *the Specifications* [2], based on the slenderness of the flange. The limit state of flange local buckling does not apply for $F_y = 36$ ksi, since all 273 WT-shapes that included in the AISC Shapes Database V14.0 have compact flanges. There are only 10 WT-shapes that have non-compact flanges in flexural compression for $F_y = 50$ ksi, they are listed in *Table 2*. These WT-shapes are excluded from this paper. Therefore, the limit state of flange local buckling is not a concern of the discussion.

$$\begin{aligned} F_{cbx_flange} &= \frac{\phi_b M_{nx}}{S_{xc}} = \frac{\phi_b (1.6 F_y S_x)}{S_{xc}} = \frac{\phi_b (1.6 F_y)}{S_{xc} / S_x} \\ &= \frac{\phi_b (1.6 F_y)}{(d - y) / y} = \frac{\phi_b (1.6 F_y)}{2.23 \sim 5.43} \\ &= \phi_b (0.29 \sim 0.72) F_y \end{aligned} \quad (10)$$

4.2. Available Flexural Stresses F_{cbx} - Design Approach 2

The very low available flexural stress in the flange ($F_{cbx} = \phi_b (0.29 \sim 0.72) F_y$) under the *limit state of yielding* as described in the Design Approach 1 is due to the lack of distinction between the compression flange yielding and tension stem yielding in Section F9 of *the Specifications* [2]. For a Tee loaded in the plane of symmetry under pure bending, the limit state of yielding is always controlled by the stress in the stem, so the distinction between the compression flange yielding and tension stem yielding is not necessary. However, as described earlier, for a Tee in compression that is eccentrically loaded from its flange, although the moment due to the connection eccentricity produces a large tensile stress in the tip of stem, the uniformly distributed compressive stress due to the applied axial load reduces the tensile stress in the stem. Therefore, the available flexural stress in the flange and in the stem should be investigated separately, and the distinction of compression flange yielding from tension stem yielding becomes necessary.

Eccentrically loaded Tees can be treated as a special case of a singly symmetric I-shaped section with the width of tension flange equaling the stem thickness, bent about their major axis

(Figure 6). The singly symmetric I-shaped members bent about their major axis are covered in Sections F4 and F5 of the *Specifications* [2] depending upon the compactness of the web. However as stated in Section F4, I-shaped members that are applicable to Section F4 may be designed conservatively using Section F5, therefore Section F5 will be used in this paper to aid the evaluation of the available critical stresses in the flange.

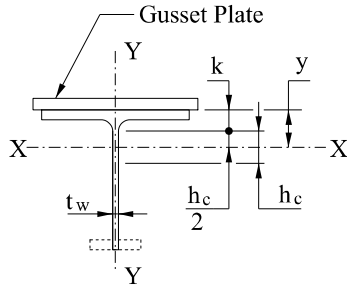


Figure 6. Singly Symmetric I-shaped Section.

For singly symmetric I-shaped members under pure flexure bent about their major axis, the nominal flexural strength, M_{nx} , shall be the lowest value obtained according to the limit states of *compression flange yielding*, *lateral-torsion buckling*, *compression local buckling*, and *tension flange yielding*.

The available critical stress in the stem according to the limit state of tension stem is the same as Approach 1,

$$F_{cbx_stem} = \phi_b (1.6 F_y) \quad (11)$$

The available critical stress in the flange according to the limit state of compression flange can be obtained based on Equation F5-1 of the *Specifications* [2],

$$M_{nx} = R_{pg} F_y S_{xc} \quad (12)$$

where, R_{pg} , the bending strength reduction factor is determined as follows:

$$R_{pg} = 1 - \frac{a_w}{1,200 + 300a_w} \left(\frac{h_c}{t_w} - 5.7 \sqrt{\frac{E}{F_y}} \right) \leq 1.0 \quad (13)$$

where, h_c , twice the distance from the centroid to the inside face of compression flange less the fillet.

$$a_w = h_c t_w / b_f t_f$$

After examining all 273 WT-shapes, it is concluded that $R_{pg} = 1.0$ for all WT-shapes. Therefore, the available critical stress in the flange is defined as:

$$F_{cbx_flange} = \frac{\phi_b M_{nx}}{S_{xc}} = \frac{\phi_b R_{pg} F_y S_{xc}}{S_{xc}} = \phi_b F_y \quad (14)$$

5. Design Example

The following example (Figure 7) demonstrates the procedure that is used by the two approaches, the procedure

used by Approach 2 is incorporated in the Microsoft Excel spreadsheet to generate the design tables.

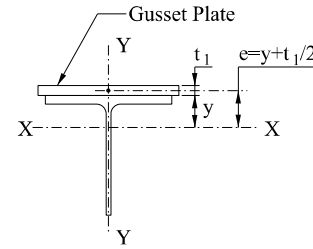


Figure 7. WT Design Example.

$KL = 120$ in.	$F_y = 36$ ksi	$E = 29,000$ ksi
$A_g = 5.17$ in. ²	$d = 6.25$ in.	$t_w = 0.300$ in.
$b_f = 6.56$ in.	$t_f = 0.520$ in.	$y = 1.30$ in.
$I_x = 16.0$ in. ⁴	$S_x = 3.23$ in. ³	$r_x = 1.76$ in.
$I_y = 12.2$ in. ⁴	$S_y = 3.73$ in. ³	$r_y = 1.54$ in.
$Z_x = 5.71$ in. ³	$Z_y = 5.73$ in. ³	$J = 0.369$ in. ⁴
$H = 0.835$	$r_o = 2.56$ in.	$t_l = 0.625$ in.
$KL/r \leq 200$	$\phi_c = 0.90$	$\Omega = 1.67$

5.1. Check Required Radius of Gyration, r_{min}

Required radius of gyration $r_{min} = KL/200 = 1.0(120)/200 = 0.60$ in. $< \min(r_x, r_y) = 1.54$ in., ok

5.2. Check for Slender Element

For uniform compression in flange – Since the flanges of all Tees are either *compact* or *non-compact elements*, there is no need to check the flange for slender element. For uniform compression in stem (Case 8, Table B4.1a, Section B4, the *Specifications* [2]),

$$\frac{d}{t_w} = \frac{6.25}{0.30} = 20.8 < \lambda_r = 0.75 \sqrt{\frac{E}{F_y}} = 0.75 \sqrt{\frac{29,000}{36}} = 21.3$$

\therefore Stem satisfies *limiting width-thickness ratios* for *non-compact elements*, and Sections E3 and E4 of the *Specifications* [2] should be used to compute the available axial compressive stresses.

5.3. Determine the Available Axial Stress, F_{ca}

5.3.1. The Critical Compressive Stress, F_{cr} , Based on the Limit State of Flexural Buckling (Section E3 of the *Specifications* [2])

Flexural buckling about the x-x axis:

$$\frac{KL}{r_x} = \frac{1.0(120)}{1.76} = 68.18$$

$$F_{ex} = \frac{\pi^2 E}{\left(\frac{KL}{r_x} \right)^2} = \frac{\pi^2 (29,000)}{68.18^2} = 61.57 \text{ ksi}$$

Since $F_y / F_{ex} = 36/61.57 = 0.585 \leq 2.25$, Equation E3-2 of

the Specifications [2] applies,

$$F_{crx} = \left[0.658^{\frac{F_y}{F_{ex}}} \right] F_y = \left[0.658^{\frac{36}{61.57}} \right] (36) = 28.18 \text{ ksi}$$

Flexural buckling about the y-y axis:

$$\frac{KL}{r_y} = \frac{1.0(120)}{1.54} = 77.92$$

$$F_{ey} = \frac{\pi^2 E}{\left(\frac{KL}{r_y} \right)^2} = \frac{\pi^2 (29,000)}{77.92^2} = 47.14 \text{ ksi}$$

$$F_{cry} = \left[0.658^{\frac{F_y}{F_{ey}}} \right] F_y = \left[0.658^{\frac{36}{47.14}} \right] 36 = 26.15 \text{ ksi}$$

5.3.2. The Critical Compressive Stress, F_{cr} , Based on the Limit States of Torsional and Flexural-Torsional Buckling (Section E4 of the Specifications [2])

$$F_{crz} = \frac{GJ}{A_g \bar{r}_0^2} = \frac{11,200(0.369)}{5.17(2.56)^2} = 121.98 \text{ ksi}$$

From Equation E4-2 of the Specifications [2],

$$F_{cr} = \left(\frac{F_{cry} + F_{crz}}{2H} \right) \left[1 - \sqrt{1 - \frac{4F_{cry}F_{crz}H}{(F_{cry} + F_{crz})^2}} \right]$$

$$= \left(\frac{26.15 + 121.98}{2(0.835)} \right) \left[1 - \sqrt{1 - \frac{4(26.15)(121.98)(0.835)}{(26.15 + 121.98)^2}} \right]$$

$$= 25.08 \text{ ksi}$$

5.3.3. The Available Axial Compressive Stress, F_{ca}

The controlling critical compressive stress, F_{cr}

$$F_{cr} = \min(F_{crx}, F_{cry}, F_{crz}) = 25.08 \text{ ksi}$$

The available axial compressive stress, F_{ra}

$$F_{ca} = \phi_c F_{cr} = 0.9(25.08) = 22.57 \text{ ksi}$$

5.4. The available Flexural Stress, F_{cbx_stem} , F_{cbx_flange}

5.4.1. The Nominal Flexural Strength, M_{nx} Based on the Limit State of Yielding for Stem in Tension (Section F9.1 of the Specifications [2])

Approach 1:

$$M_{nx} = \min[F_y Z_x, 1.6 M_{yx} = 1.6 F_y S_x]$$

$$= \min[36(5.71), 1.6(36)(3.23)]$$

$$= \min[205.56, 186.05] = 186.05 \text{ kip-in.}$$

The available flexural stress, F_{cbx_stem} , F_{cbx_flange}

$$F_{cbx_stem} = \frac{\phi_b M_{nx}}{S_x} = \frac{0.9(186.05)}{3.23} = 51.84 \text{ ksi}$$

$$F_{cbx_flange} = \frac{\phi_b M_{nx}}{S_{xc}} = \frac{0.9(186.05)}{12.31} = 13.60 \text{ ksi}$$

Approach 2:

The available flexural stress, F_{cbx_stem} based on the limit state of yielding in stem that in tension,

$$F_{cbx_stem} = \phi_b 1.6 F_y = 0.9(1.6)(36) = 51.84 \text{ ksi}$$

The available flexural stress, F_{cbx_flange} based on the limit state of yielding in flange that in compression

$$F_{cbx_flange} = \phi_b F_y = 0.9(36.00) = 32.40 \text{ ksi}$$

5.4.2. The Nominal Flexural Strength, M_{nx} Based on the Limit State of Lateral-Torsional Buckling (Section F9.2 of the Specifications [2])

Assuming stem in tension,

$$B = 2.3 \left(\frac{d}{L_b} \right) \sqrt{\frac{I_y}{J}} = 2.3 \left(\frac{6.25}{120} \right) \sqrt{\frac{12.2}{0.369}} = 0.69$$

$$M_{nx} = M_{cr} = \frac{\pi \sqrt{EI_y GJ}}{L_b} [B + \sqrt{1 + B^2}]$$

$$= \frac{\pi \sqrt{29,000(12.2)(11,200)(0.369)}}{120} \times [0.69 + \sqrt{1 + 0.69^2}]$$

$$= 1905.03 \text{ kip-in.}$$

The available flexural stresses, F_{cbx_stem} and F_{cbx_flange}

$$F_{cbx_stem} = \frac{\phi_b M_{nx}}{S_x} = \frac{0.9(1905.03)}{3.23} = 530.8 \text{ ksi, not control;}$$

$$F_{cbx_stem} = \frac{\phi_b M_{nx}}{S_{xc}} = \frac{0.9(1905.03)}{12.31} = 138.2 \text{ ksi, not control}$$

5.4.3. The Nominal Flexural Strength, M_{nx} Based on the Limit State of Flange Local Buckling (Section F9.3 of the Specifications [2])

Check the compactness of flange for flexure,

$$\frac{b_f}{2t_f} = \frac{6.56}{2(0.52)} = 6.3 < \lambda_r = 1.0 \sqrt{\frac{E}{F_y}} = 1.0 \sqrt{\frac{29,000}{36}} = 28.4$$

$$\frac{b_f}{2t_f} = \frac{6.56}{2(0.52)} = 6.3 < \lambda_p = 0.38 \sqrt{\frac{E}{F_y}}$$

$$= 0.38 \sqrt{\frac{29,000}{36}} = 10.8$$

∴ Flange is compact, and the limit state of flange local buckling does not apply.

5.4.4. The Controlling Available Flexural Stresses, F_{cbx_stem} and F_{cbx_flange}

Approach 1:

$$F_{cbx_stem} = 51.84 \text{ ksi}$$

$$F_{cbx_flange} = 13.60 \text{ ksi}$$

Approach 2:

$$F_{cbx_stem} = 51.84 \text{ ksi}$$

$$F_{cbx_flange} = 32.40 \text{ ksi}$$

5.5. The Available Flexural Stress, F_{cby}

Since there is no flexural moment about axis y-y, in this example, calculation of F_{cby} is not required (Section F6 of the Specifications [2])

5.6. The Required Flexural Moment Due to Axial Load and Eccentricity of Connection, M_{rx}

$$M_{rx} = B_{1x} M_{ecc} = B_{1x} P_r (y + t_1 / 2)$$

$$= B_{1x} P_r (1.3 + 0.625 / 2)$$

$$= (1.6125) B_{1x} P_r \text{ kip-in.}$$

where, B_1 – 2nd-Order effect based on Appendix Equation A-8-3 of the Specifications [2],

$$B_1 = \frac{C_m}{1 - \alpha P_r / P_{el}} \geq 1.0$$

where, $\alpha = 1.0$ (LRFD); 1.6 (ASD)

$C_m = 1.0$ (conservative)

$$P_{el} = \frac{\pi^2 0.8 \tau_b EI}{(K_1 L)^2}$$

$$P_{el} = \frac{\pi^2 0.8 \tau_b EI}{(K_1 L)^2}$$

$$\tau_b = 1.0 \text{ if } \alpha P_r / (F_y A_g) \leq 0.5$$

$$\tau_b = \frac{4\alpha P_r}{F_y A_g - \alpha P_r} \text{ if } \alpha P_r / (F_y A_g) > 0.5$$

$$P_{elx} = \frac{\pi^2 0.8 \tau_b EI_x}{(K_1 L)^2} = \frac{\pi^2 (0.8) \tau_b (29,000)(16.0)}{(1.0(120))^2}$$

$$= 254.42 \tau_b$$

$$B_{1x} = \frac{C_m}{1 - \alpha P_r / P_{elx}} = \frac{1.0}{1 - 1.0(P_r) / 254.42 \tau_b}$$

$$= \frac{254.42 \tau_b}{254.42 \tau_b - P_r}$$

The required flexural moment due to axial load and eccentricity of connection, M_{rx}

$$M_{rx} = (1.6125) B_{1x} P_r$$

$$= (1.6125 P_r) \left(\frac{254.42 \tau_b}{254.42 \tau_b - P_r} \right) \text{ kip-in.}$$

5.7. Interaction of Flexure and Compression

Actual axial stress, f_a

$$f_a = \frac{P_r}{A_g} = \frac{P_r}{5.17} \text{ ksi}$$

Actual flexural stress f_{bx} , due to M_{rx}

$$f_{bx-flange} = \frac{M_{rx}}{S_{xc}} = \frac{(1.6125 P_r) \left(\frac{254.42 \tau_b}{254.42 \tau_b - P_r} \right)}{12.31}$$

$$f_{bx-stem} = \frac{M_{rx}}{S_x} = \frac{(1.6125 P_r) \left(\frac{254.42 \tau_b}{254.42 \tau_b - P_r} \right)}{3.23}$$

Interaction at tip of the stem,

$$\left| \frac{f_{ra}}{F_{ca}} - \frac{f_{rbx_stem}}{F_{cbx_stem}} \right| = \left| \frac{f_{ra}}{22.57} - \frac{f_{rbx_stem}}{51.84} \right| \leq 1.0$$

Solve above equation, $P_r = 944.42$ kips, not control.

Interaction at edge of the flange – Approach 1

$$\left| \frac{f_{ra}}{F_{ca}} + \frac{f_{rbx_flange}}{F_{cbx_flange}} \right| = \left| \frac{f_{ra}}{22.57} + \frac{f_{rbx_flange}}{13.60} \right| \leq 1.0$$

Solve above equation, $P_r = 48.78$ kips

Interaction at edge of the flange – Approach 2

$$\left| \frac{f_{ra}}{F_{ca}} + \frac{f_{rbx_flange}}{F_{cbx_flange}} \right| = \left| \frac{f_{ra}}{22.57} + \frac{f_{rbx_flange}}{32.40} \right| \leq 1.0$$

Solve above equation, $P_r = 70.56$ kips

5.8. Compressive Strength

The Design Compressive Strength (LRFD), $\phi_c P_n$

Approach 1:

$$\phi_c P_n = P_r = 48.78 \text{ kips}$$

Approach 2:

$$\phi_c P_n = P_r = 70.56 \text{ kips}$$

The Allowable Compressive Strength (ASD), P_n/Ω

Approach 1:

$$P_n/\Omega = (P_r/\phi_c)/\Omega = (48.78/0.9)/1.67 = 32.45 \text{ kips}$$

Approach 2:

$$P_n/\Omega = (P_r/\phi_c)/\Omega = (70.56/0.9)/1.67 = 46.95 \text{ kips}$$

6. Discussions

6.1. Design Approaches

As illustrated in the design example above, for an eccentrically loaded WT6x17.5 in compression with an unbraced length of 10 ft. and an eccentricity of 1.6125", the axial capacity of 70.56 kips based on Approach 2 is much higher than the capacity of 48.78 kips based on Approach 1.

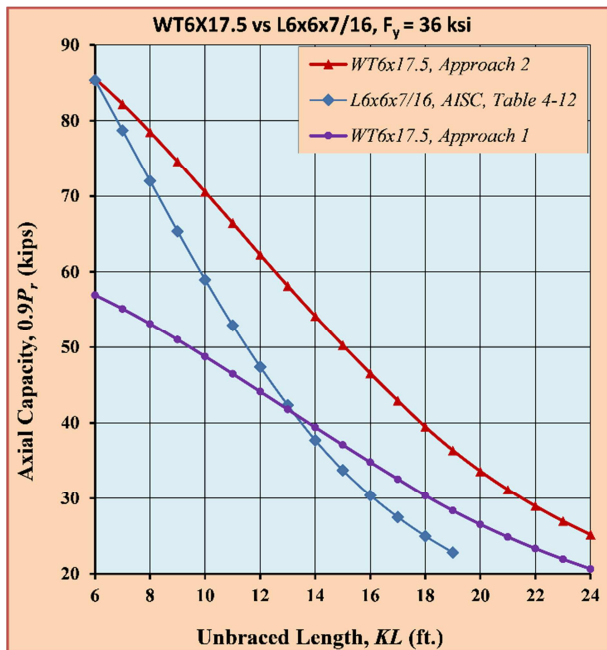


Figure 8. Axial Capacity Comparison of WT-shape and Angle of the Similar Weight.

This can be further observed from Figure 8 which shows that with unbraced lengths between 6 ft. and 24 ft., the capacities of WT6x17.5 determined by Approach 1 are much less than the capacities determined by Approach 2. The capacities of WT6x17.5 determined by Approach 1 are even less than the capacities of the single angle L6x6x7/16 for unbraced lengths less than 13 ft., on the other hand, the capacities of the WT6x17.5 determined by Approach 2 are larger than the capacities of the single angle L6x6x7/16, the

larger the unbraced length, the greater the difference in capacities. This is further evidence that Approach 1 results in inefficient designs. The same conclusion was drawn by Galambos [7] that "the ASIC-type approach can be quite conservative, especially for tee-shapes". The "AISC-type approach" by Galambos is identified as Approach 1 in this paper.

Tito [9] performed tests on two eccentrically loaded WT5x11 braces with the compressive force applied through 1/2" gusset plates, the WT shapes were cut from a Gr. 50 W10x22 and 15 ft in length. Both tests showed the stem tip reached tension yielding stress at 27.4 kips and the flange reached compression yielding after large deflections of the braces and sustaining the maximum load of 29.3 kips. With a resistance factor $\phi_c = 0.90$ the axial compression strength is 26.37 kips, which is very close to the available strength of 27.8 kips from the design tables presented at the end of this paper. It should be noted that the tested WT shapes have an initial 5/8" camber, which exceeds the allowed mill straightness tolerance of 3/8" per Table 1-54 of the Manual [1].

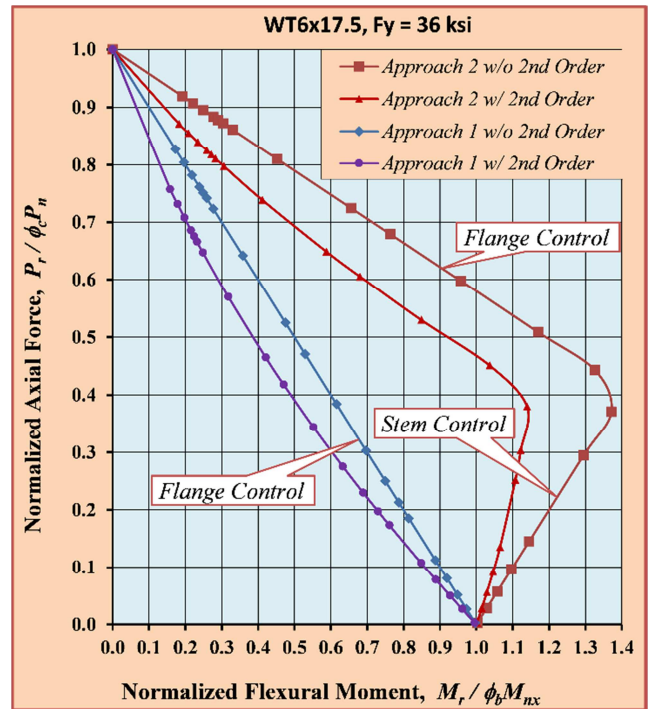


Figure 9. WT-shape Interaction Curve: Axial Force vs. Moment.

Figure 9 displays the normalized axial capacity vs. flexural capacity interaction diagram of the same member, where $\phi_c P_n = \phi_c F_{cr} A_g = (0.9)(25.08)(5.17) = 116.69$ kips, and $\phi_b M_{nx} = \phi_b (1.6) F_y S_x = (0.90)(1.6)(36)(3.23) = 167.45$ kip-in. The interaction diagram based on Approach 1 is in linear variation when the second order effect is not considered, shows that the stress ratio in the flange controls the design for entire curve; on the other hand, with Approach 2, the stress ratio in the flange controls the design when $P_r/\phi_c P_n > 0.4$; the controlling stress ratio transitions to stem controls when $P_r/\phi_c P_n < 0.4$. The interaction curves shown in Figure 9 are very much like the interaction curves presented by Galambos [7].

The benefit of Approach 2 can be further visualized with interaction diagram of axial compressive stress vs. flexural compressive stress in flange as shown in Figure 10. With Approach 1 where stress ratio in flange controls the design, the flexural compressive stress in flange is limited to 13.40 ksi; however, with Approach 2 when the stress ratio in the flange controls the design, the flexural compressive stress in the flange in the trend reaches $0.9F_y$, until the controlling stress ratio transitions from flange controls to stem controls.

Figure 10 is similar as Figure C-H2.2 shown in Commentary H2 of the Specifications [2] except that Figure C-H2.2 is for a WT when the stem in flexural compression is combined with axial tension, or an eccentrically loaded WT in tension.

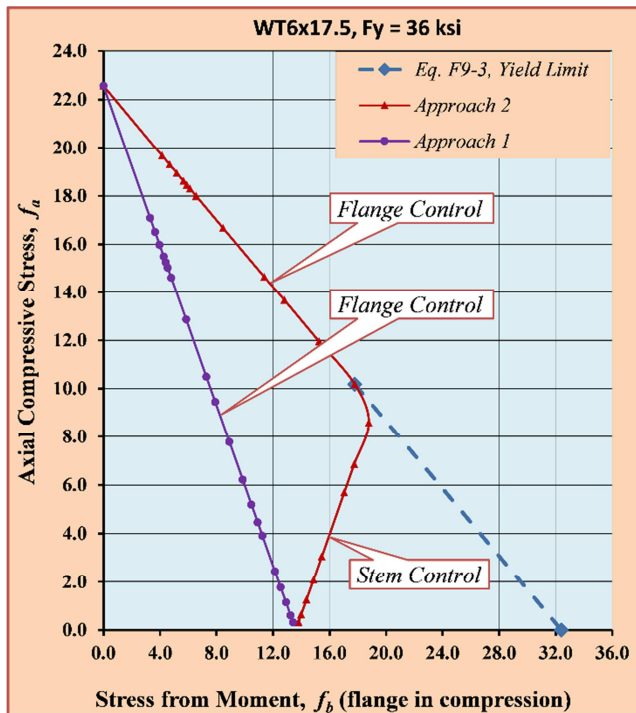


Figure 10. WT-shape Axial Compressive Stress vs. Flexural Compressive Stress in Flange.

6.2. Available Flexural Stresses in Flanges

As discussed in the Design Considerations, the nominal flexural strength M_{nx} shall be the lowest value obtained according to the limit states of yielding, lateral torsional buckling, and flange local buckling, and the available flexural stress in flange F_{cbx_flange} can be calculated based on Equation (5).

Excluding ten (10) WT-shapes, flange local buckling is not applicable to WT-shapes. The available stresses in the flange based on the remaining two limit states – yielding and lateral torsional buckling are presented in Figure 11. It can be concluded that for WT6x17.5 with Grade 36 steel and unbraced lengths as shown, the yielding, rather than lateral torsional buckling, controls the available stresses in the flanges. Therefore, in order to design a Tee member more efficiently, it is critical to distinguish the section modulus for the flange and stem when determining the yielding strength of the Tee under combined axial compression and flexural compression on the flanges.

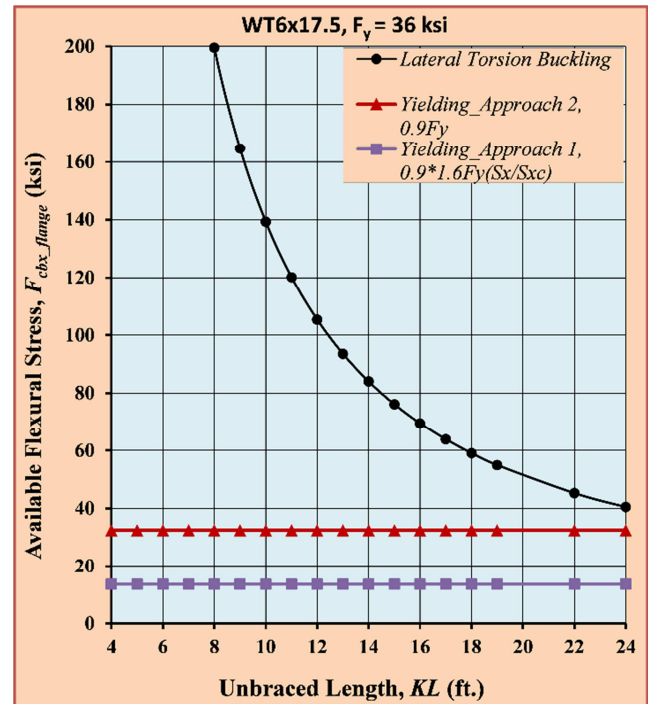


Figure 11. Available Flexural Stresses in Flanges.

7. Finite Element Analyses

As discussed previously, Approach 2 yields a greater and much needed capacity of an eccentrically loaded WT-shape. The member's resistances derived from design Approach 2 were validated through nonlinear Finite Element (FE) analysis using LUSAS Bridge software [6], which considers buckling behavior, second-order effects, geometrically nonlinear (initial imperfection), and material nonlinearity (yielding) of the member. Initial imperfection can be considered the same as the mill straightness tolerance for camber or sweep. According to Table 1-54 for W-shapes or H-shapes, and Table 1-56 for WT-shapes of the Manual [1], that is $\frac{1}{8} \left(\frac{\text{Total Length, ft}}{5} \right)$, the results of the FE analyses are discussed below.

7.1. Finite Element Analysis of Centrally Loaded Members

AISC [1] provides axial capacities for centrally loaded W-shapes and WT-shapes in compression. In order to test the FE modeling techniques and serve as a benchmark to analyze eccentrically loaded WT-sections, FE analyses were first performed to analyze centrally loaded doubly symmetric I-shape W14x82 and centrally loaded singly symmetric WT6x17.5. Two element types were utilized in these analyses: three Dimensional Semiloof Cross Section Beam (BXL4) and quadrilateral Thick Shell (QTS8), elements used in the study are sufficiently refined and not to be discussed in this paper [5]. Figure 12 shows axial capacities of W14x82 obtained from FE analysis and from Table 4-1 of the Manual [1]; Figure 13 shows axial capacities of WT6x17.5 obtained from FE analysis and from Table 4-7 of the Manual [1]. Both Figure 12 and Figure 13 indicate that finite element analysis using both beam element

and shell element yields very similar capacities for both methods for doubly symmetric I-shape and singly symmetric WT-shape. It can also be concluded that finite element analysis can very accurately predict the axial capacity of both I-shapes and WT-shapes with large unbraced length, and that when the unbraced length is small, the axial capacities obtained from Table 4-1 and Table 4-7 of the *Manual* [1] are conservative; the conservativeness is greater with WT-shapes than with I-shapes.

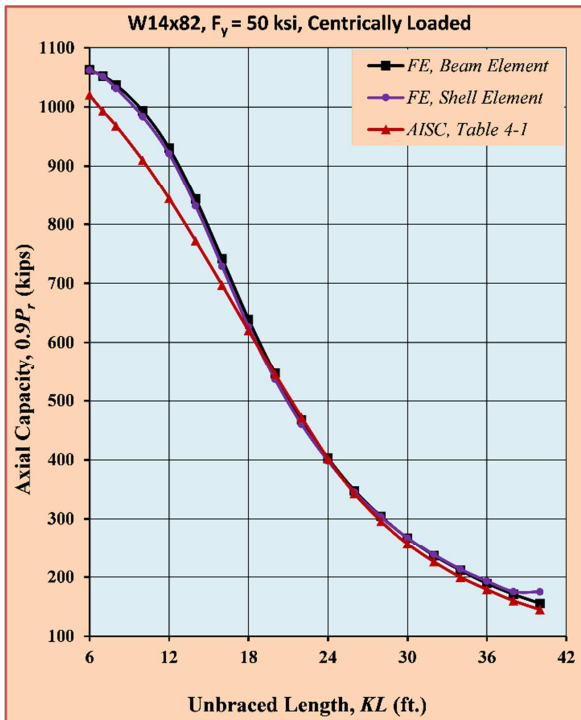


Figure 12. Axial Capacities of W14x89.

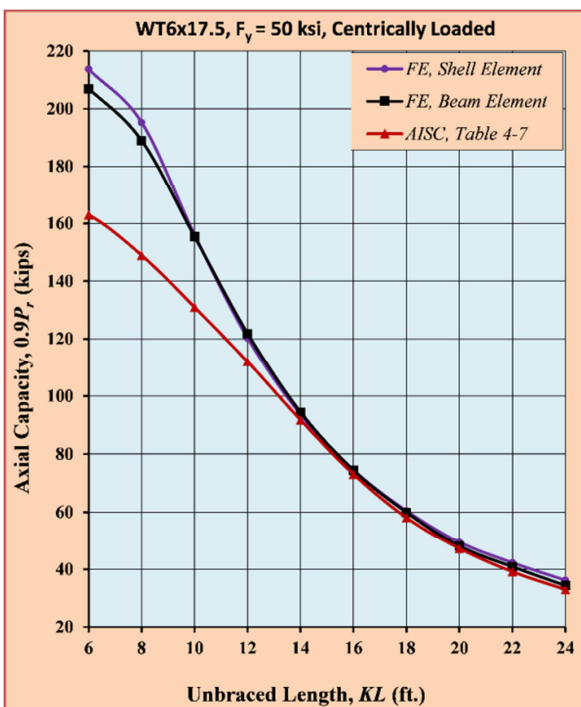


Figure 13. Axial Capacities of WT6x17.5.

7.2. Finite Element Analysis of Eccentrically Loaded Tees

Since finite element nonlinear analysis using either beam element or shell element yields similar capacities of centrally loaded Tees, shell element (QTS8) was used to investigate eccentrically loaded WT - shapes, flange elements are taken at mid-thickness of the flange. The following discussion is for: WT6x17.5 with unbraced length of 10 feet, Gr. 36 steel, eccentrically loaded with an eccentricity of 1.6125", and the initial imperfection is 0.125".

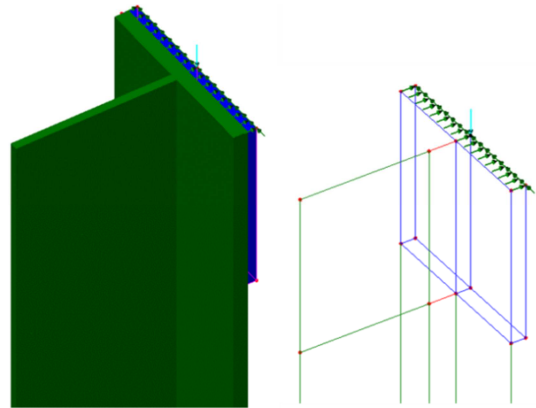


Figure 14. Axial Load at 1.6125" from NA of Tee.

Eccentricity: To apply the axial load at 1.6125" from the neutral axis (NA) of WT6x17.5, solid elements (HX20) are incorporated to both ends of the member in the model as shown in Figure 14. A concentrated load is applied in the vertical (Z-axis) at a node of the solid element, while outside edges of solid elements are simply supported in both the X- and Y- axes.

Buckling Modes: Figure 15 presents the first three buckling modes with eigenvalues of 312.11 kips, 461.64 kips, and 1155.98 kips respectively. The first mode is usually of interest and the initial imperfection of 0.125" is started with the deformed mesh from buckling mode 1.

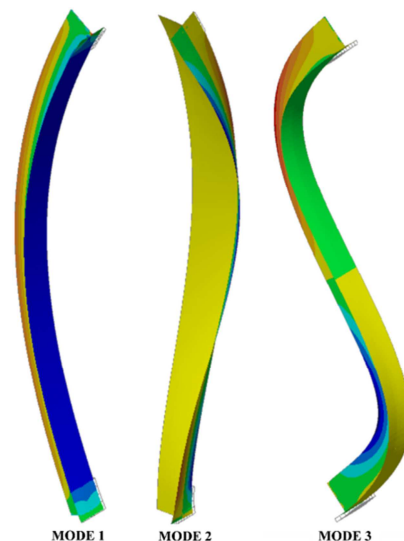


Figure 15. Buckling Modes of Eccentrically Loaded Tee.

Nominal Axial Capacity, Stress Distributions and Load vs. Displacement Curve: The nominal axial capacity based on nonlinear finite analysis is $P_r = 87.23$ kips, therefore, the factored available strength $\phi_c P_r = 0.90 \times 87.23 = 78.51$ kips, which is slightly larger than 70.56 kips from the calculation based on Approach 2.

Stress distribution along the stem (local y-y axis) at mid-height of the tee member is shown in Figure 16 and 17. Figure 16 shows the stress distribution at the maximum load of $P_r = 87.23$ kips. The averaged nodal tensile stresses within

40% of stem reach yield stress of 36 ksi (F_y), while the compressive stresses in flange are slightly lower than F_y . Figure 17 shows the stress distribution before and after the load reaches the maximum load of P_r , the maximum tensile stress in the stem reaches F_y when the load is at $0.80P_r$, while the compressive stresses in the flange is only 24 ksi. With the increase of applied load, more area of the stem is yielded, and stress in flange is increased, the compressive stress in flange eventually reaches the F_y .

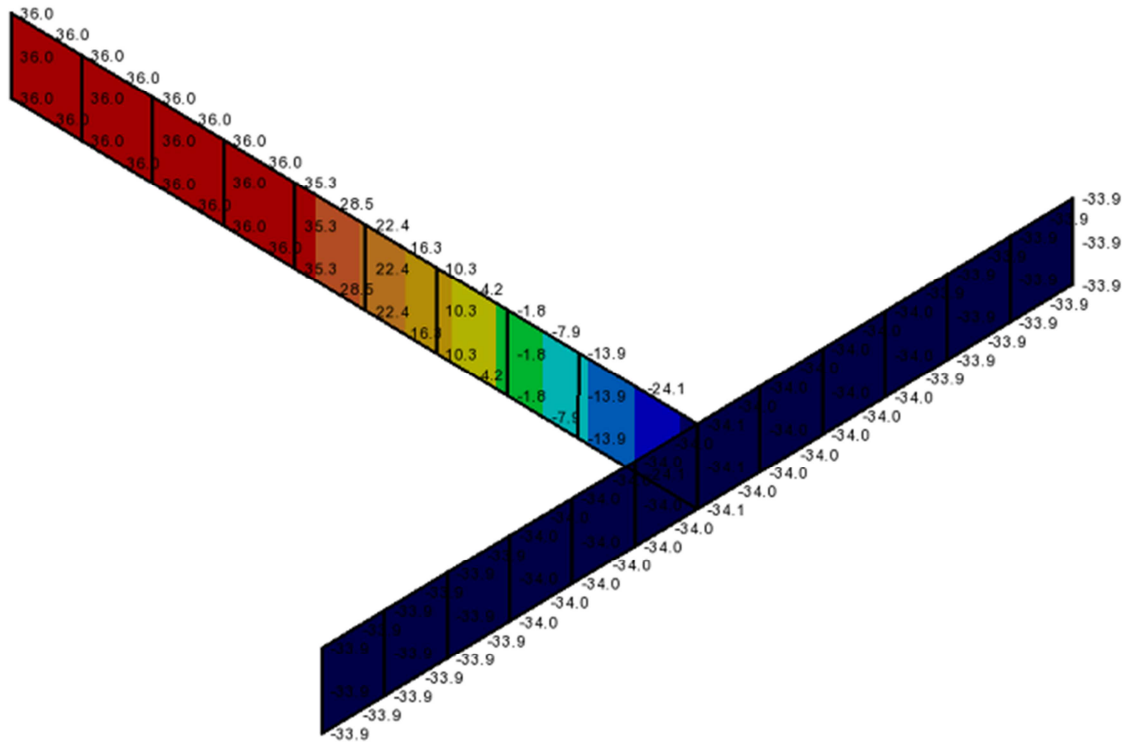


Figure 16. Stress Distribution at $P_r = 87.23$ kips.

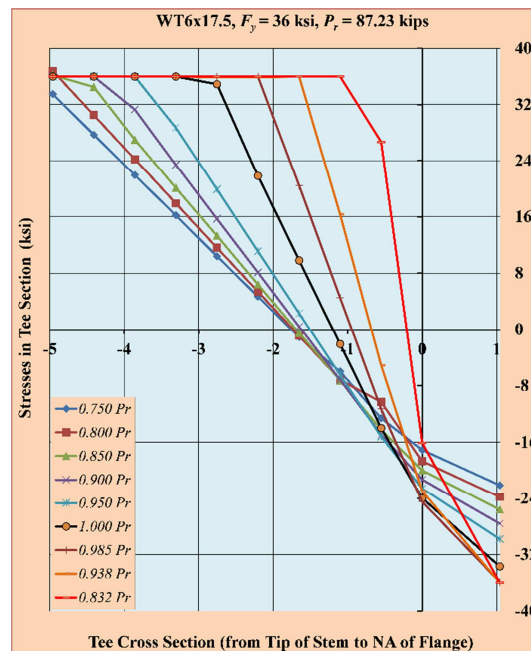


Figure 17. Stress Distribution before and after $1.0P_r$.

Load vs. mid-height displacement curve is shown in *Figure 18*. Linear variation is observed when the applied load is less than $0.80P_r$, and the stresses in the WT6x17.5 are less than F_y (also see *Figure 17*). The load vs. displacement curve indicates continual strength gain when more area of the stem reaches F_y . A 1.0-inch displacement is noted when WT6x17.5 reaches its ultimate strength.

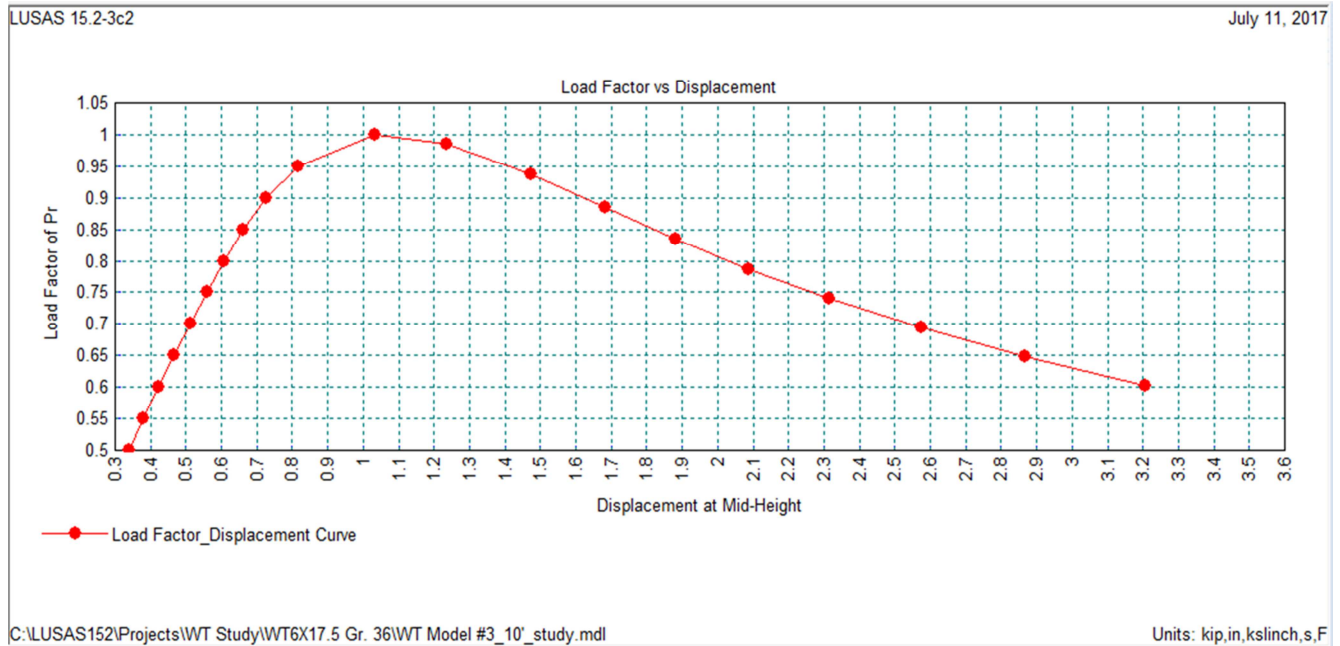


Figure 18. Load Factor of P_r vs. Displacement.

7.3. Axial Capacity Comparison Between Approach 2 and Nonlinear Finite Element Analysis

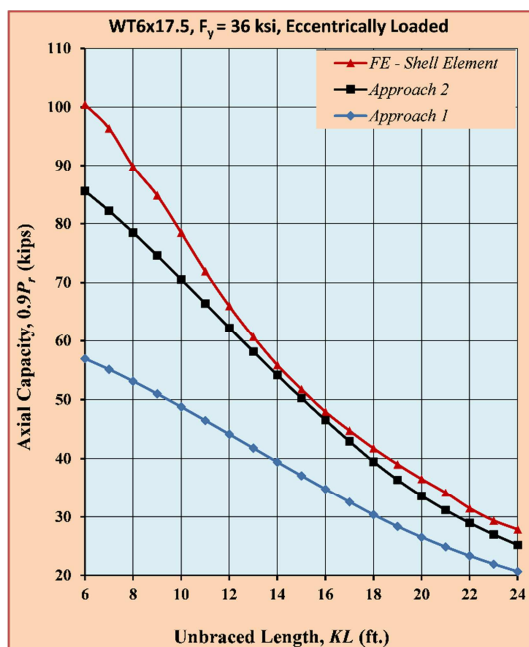


Figure 19. Axial Capacities of WT6x17.5.

The results of the finite element analysis and calculated axial capacity of WT6x17.5 based on both approaches discussed in the paper are presented in *Figure 19*. As indicated previously, while the axial capacities of eccentrically loaded

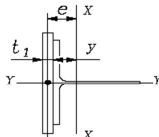
WT-shapes based on Approach 2 are consistently larger than those based on Approach 1, they are still less than the results from this finite element analysis and are therefore conservative. The conservativeness of the axial capacity of eccentrically loaded WT-shapes based on Approach 2 is in line with the axial capacity of centrally loaded WT-shapes per Table 4-7 of the *Manual* [1], as shown in *Figure 13*.

8. Conclusions

This paper proposed an alternate approach (Approach 2) allowed for by Section Comm. H2. of the *Specifications* [2] to design the eccentrically loaded WT-shapes in Compression, and the calculated strengths based on Approach 2 are larger and more reasonable than those based on Section H2 of the *Specifications* [2] (Approach 1). Extensive Finite Element Nonlinear analyses have been employed to validate the proposed approach. Design tables to facilitate implementation of the procedure of Approach 2 have also been developed.

Only a few experimental tests on eccentrically loaded WT-shapes in compression are available. The capacities of two 15 ft long WT15x11 braces tested by Tito [9] agree very well with the calculated capacities based on the proposed approach; the percent difference between the experimental factored average capacity and the factored capacity predicted by Approach 2 is 94.85%.

The results from finite element analyses and experimental tests clearly indicate that the proposed approach is quite accurate in predicting the ultimate capacity of eccentrically loaded WT-shapes in compression.

<div></div> <div>Available Strength in Axial Compression, Kips Eccentrically Loaded WTs</div>															
Design	P_n/Ω_c	$\phi_c P_n$	P_n/Ω_c	$\phi_c P_n$	P_n/Ω_c	$\phi_c P_n$	P_n/Ω_c	$\phi_c P_n$	P_n/Ω_c	$\phi_c P_n$	P_n/Ω_c	$\phi_c P_n$	P_n/Ω_c	$\phi_c P_n$	
	ASD	LRFD	ASD	LRFD	ASD	LRFD	ASD	LRFD	ASD	LRFD	ASD	LRFD	ASD	LRFD	
Shape	WT8x														
	50.0		44.5		38.5		33.5		28.5		25 ^S		22.5 ^S		
F_y	36 ksi														
Effective Length KL (ft)	6	167.5	251.8	153.1	230.1	134.3	201.8	119.6	179.8	89.8	134.9	78.9	118.6	68.0	102.3
	7	164.2	246.7	150.0	225.4	131.4	197.4	117.1	176.1	87.1	131.0	77.0	115.7	66.5	100.0
	8	160.4	241.0	146.4	220.1	128.2	192.7	114.3	171.8	84.2	126.6	74.6	112.1	64.6	97.2
	9	156.2	234.7	142.6	214.3	124.8	187.6	111.2	167.2	81.0	121.8	71.8	107.9	62.4	93.9
	10	151.3	227.4	138.4	208.0	121.1	182.0	107.9	162.2	77.6	116.7	68.8	103.4	60.0	90.2
	11	146.2	219.7	133.6	200.8	117.2	176.1	104.4	156.9	74.1	111.4	65.6	98.6	57.3	86.2
	12	140.8	211.7	128.6	193.3	112.7	169.4	100.7	151.3	70.4	105.9	62.3	93.6	54.6	82.0
	13	135.4	203.5	123.5	185.6	108.1	162.5	96.5	145.1	66.7	100.3	58.9	88.5	51.7	77.7
	14	129.8	195.1	118.3	177.8	103.4	155.5	92.2	138.6	62.9	94.6	55.4	83.3	48.8	73.3
	15	124.3	186.8	113.1	170.0	98.8	148.4	87.9	132.2	59.1	88.8	52.0	78.1	45.8	68.9
	16	118.7	178.4	107.9	162.2	94.1	141.5	83.6	125.7	55.3	83.1	48.5	72.9	42.9	64.5
	17	113.1	170.0	102.7	154.4	89.5	134.4	79.4	119.4	51.5	77.5	45.1	67.8	40.0	60.1
	18	107.7	161.9	97.7	146.8	85.0	127.7	75.3	113.2	47.7	71.7	41.6	62.6	37.1	55.8
	20	97.3	146.3	88.1	132.4	76.4	114.8	67.5	101.4	40.8	61.4	35.6	53.5	31.7	47.6
22	87.6	131.6	79.0	118.7	68.3	102.7	60.2	90.4	35.3	53.0	30.7	46.2	27.3	41.0	
24	78.5	118.0	70.7	106.2	60.9	91.6	53.5	80.4	30.7	46.1	26.7	40.2	23.7	35.7	
26	70.1	105.4	63.0	94.7	54.2	81.4	47.4	71.3	26.9	40.5	23.4	35.2	20.8	31.2	
F_y	50 ksi														
Effective Length KL (ft)	6	226.4	340.2	206.4	310.2	174.8	262.7	142.5	214.2	116.4	175.0	95.6	143.7	80.1	120.3
	7	220.2	331.0	200.7	301.6	171.3	257.5	140.2	210.7	112.4	169.0	92.7	139.4	78.0	117.3
	8	213.3	320.6	194.3	292.0	167.1	251.2	137.4	206.5	107.7	161.9	89.3	134.3	75.5	113.5
	9	205.9	309.4	187.4	281.6	162.2	243.7	134.1	201.5	102.5	154.0	85.4	128.4	72.6	109.1
	10	197.2	296.4	180.1	270.6	156.5	235.1	130.2	195.7	96.9	145.6	81.2	122.0	69.3	104.2
	11	188.3	283.0	171.8	258.2	149.8	225.1	125.7	189.0	91.1	136.8	76.7	115.3	65.8	98.9
	12	179.3	269.4	163.3	245.5	142.2	213.8	120.6	181.2	85.1	127.9	72.1	108.4	62.1	93.4
	13	170.1	255.7	154.7	232.5	134.5	202.2	114.6	172.2	79.1	119.0	67.4	101.4	58.4	87.8
	14	160.9	241.9	146.2	219.8	127.0	190.9	108.5	163.0	73.1	109.9	62.8	94.3	54.6	82.1
	15	152.0	228.5	137.9	207.3	119.7	179.9	102.5	154.1	67.2	101.0	58.1	87.3	50.9	76.4
	16	143.3	215.4	129.9	195.2	112.5	169.1	96.7	145.3	61.4	92.2	53.5	80.3	47.1	70.8
	17	134.9	202.8	122.0	183.4	105.6	158.8	91.0	136.8	56.1	84.3	48.9	73.5	43.4	65.2
	18	126.8	190.6	114.6	172.2	99.0	148.8	85.5	128.6	51.4	77.3	44.8	67.4	39.7	59.7
	20	111.6	167.8	100.6	151.2	86.7	130.3	75.3	113.2	43.6	65.5	38.0	57.1	33.7	50.6
22	97.8	147.0	87.9	132.1	75.6	113.6	66.1	99.3	37.4	56.2	32.6	48.9	28.8	43.3	
24	85.8	129.0	77.0	115.7	66.1	99.4	57.8	86.8	32.3	48.6	28.2	42.3	24.9	37.4	
26	75.9	114.0	68.0	102.2	58.3	87.6	50.8	76.4	28.2	42.4	24.5	36.9	21.7	32.6	
Properties															
A_g (in. ²)	14.70		13.10		11.30		9.81		8.39		7.37		6.63		
γ_{min} (in.)	2.28		2.27		2.24		2.22		1.60		1.59		1.57		
ASD	LRFD		^S Shape is slender for compression $t_1 = \text{Roundup}(t_{flange} / 0.125") \times 1/8$												
$\Omega_c = 1.67$	$\phi_c = 0.9$		Notes: Heavily lines indicates KL/r equal to or greater than 120, 140, & 200 respectively Stem of the Tee orients horizontally												

Available Strength in Axial Compression, Kips

Eccentrically Loaded WTs

Design	P_n/Ω_c	$\phi_c P_n$	P_n/Ω_c	$\phi_c P_n$	P_n/Ω_c	$\phi_c P_n$	P_n/Ω_c	$\phi_c P_n$	P_n/Ω_c	$\phi_c P_n$	P_n/Ω_c	$\phi_c P_n$	P_n/Ω_c	$\phi_c P_n$											
	ASD	LRFD	ASD	LRFD	ASD	LRFD	ASD	LRFD	ASD	LRFD	ASD	LRFD	ASD	LRFD											
Shape	WT7x	30.5	26.5	24.0	21.5 ^s	19 ^s	17 ^s	15 ^s																	
F_y	36 ksi																								
Effective Length KL (ft)	6	106.8	160.5	89.3	134.2	82.8	124.4	71.2	107.0	59.0	88.7	50.3	75.6	41.2	62.0										
	7	102.9	154.6	86.5	130.1	80.2	120.5	69.6	104.6	57.4	86.3	49.1	73.8	40.4	60.7										
	8	98.7	148.3	83.5	125.5	77.3	116.2	67.6	101.6	55.4	83.3	47.7	71.6	39.3	59.1										
	9	94.2	141.7	80.2	120.5	74.2	111.6	65.2	98.0	53.2	80.0	45.9	69.0	38.0	57.1										
	10	89.6	134.7	76.7	115.3	71.0	106.7	62.5	94.0	50.8	76.3	44.0	66.1	36.5	54.9										
	11	84.9	127.6	73.1	109.9	67.6	101.7	59.7	89.7	48.2	72.5	41.9	63.0	34.9	52.5										
	12	80.0	120.3	69.5	104.4	64.2	96.5	56.8	85.3	45.6	68.6	39.7	59.7	33.2	49.9										
	13	75.3	113.1	65.8	98.9	60.8	91.3	53.7	80.8	43.0	64.6	37.5	56.4	31.4	47.2										
	14	70.6	106.1	62.1	93.4	57.4	86.2	50.8	76.3	40.3	60.6	35.3	53.0	29.6	44.5										
	15	66.1	99.4	58.6	88.0	54.0	81.2	47.8	71.9	37.6	56.5	33.1	49.7	27.8	41.7										
	16	61.8	92.8	55.0	82.7	50.8	76.3	45.0	67.6	35.0	52.6	30.8	46.3	25.9	39.0										
	17	57.6	86.6	51.6	77.5	47.6	71.6	42.2	63.4	32.5	48.8	28.7	43.1	24.1	36.2										
	18	53.7	80.7	48.3	72.6	44.6	67.0	39.5	59.4	30.0	45.1	26.6	39.9	22.3	33.6										
	20	46.5	69.8	42.2	63.4	38.9	58.5	34.5	51.9	25.6	38.4	22.6	34.0	19.1	28.6										
	22	40.1	60.3	36.7	55.2	33.8	50.8	30.0	45.1	22.0	33.1	19.5	29.3	16.4	24.7										
	24	35.0	52.6	32.1	48.3	29.5	44.3	26.2	39.3	19.1	28.8	16.9	25.4	14.3	21.4										
	26	30.8	46.2	28.3	42.5	26.0	39.0	23.0	34.6																
F_y	50 ksi																								
Effective Length KL (ft)	6	137.0	206.0	115.9	174.1	102.2	153.6	84.8	127.4	70.1	105.4	57.9	87.1	46.4	69.8										
	7	133.2	200.2	111.8	168.1	99.1	148.9	82.6	124.2	67.9	102.0	56.4	84.8	45.4	68.2										
	8	126.6	190.3	107.0	160.9	95.2	143.1	79.9	120.1	65.3	98.1	54.6	82.0	44.1	66.3										
	9	119.2	179.2	101.7	152.9	90.9	136.6	76.7	115.4	62.2	93.6	52.4	78.7	42.6	64.0										
	10	111.5	167.6	96.1	144.5	86.2	129.5	73.2	110.0	59.0	88.7	49.9	75.1	40.8	61.3										
	11	103.9	156.2	90.3	135.8	81.2	122.1	69.4	104.3	55.6	83.5	47.3	71.1	38.8	58.4										
	12	96.5	145.1	84.6	127.2	76.3	114.6	65.5	98.4	52.1	78.3	44.6	67.1	36.8	55.2										
	13	89.4	134.3	79.0	118.7	71.4	107.3	61.6	92.5	48.6	73.0	41.9	62.9	34.6	52.0										
	14	82.5	124.0	73.4	110.4	66.6	100.1	57.7	86.7	45.1	67.8	39.1	58.7	32.4	48.7										
	15	76.1	114.3	68.1	102.4	62.0	93.2	53.9	81.0	41.7	62.7	36.3	54.6	30.2	45.5										
	16	70.0	105.2	63.1	94.8	57.6	86.6	50.3	75.6	38.4	57.7	33.6	50.5	28.1	42.2										
	17	64.3	96.7	58.3	87.7	53.4	80.2	46.8	70.4	35.2	52.8	31.0	46.6	25.9	39.0										
	18	58.9	88.6	53.9	81.0	49.4	74.3	43.5	65.4	32.2	48.4	28.4	42.7	23.9	35.8										
	20	50.0	75.1	45.9	69.0	42.2	63.4	37.4	56.2	27.2	40.9	24.0	36.1	20.2	30.3										
	22	42.9	64.5	39.5	59.4	36.3	54.5	32.1	48.3	23.3	35.0	20.5	30.9	17.3	25.9										
	24	37.2	55.9	34.3	51.6	31.5	47.3	27.9	41.9	20.1	30.3	17.7	26.6	14.9	22.4										
	26	32.6	49.0	30.1	45.3	27.6	41.5	24.4	36.7																
Properties																									
A_g (in. ²)	8.96		7.80		7.07		6.31		5.58		5.00		4.42												
γ_{min} (in.)	1.80		1.88		1.88		1.86		1.55		1.53		1.49												
ASD	LRFD		^s Shape is slender for compression $t_1 = \text{Roundup}(t_{flange} / 0.125") \times 1/8$																						
$\Omega_c = 1.67$	$\phi_c = 0.9$		Notes: Heavy lines indicates KL/r equal to or greater than 120, 140, & 200 respectively Stem of the Tee orientates horizontally																						

Available Strength in Axial Compression, Kips

Eccentrically Loaded WT's

Design	P_n/Ω_c	$\phi_c P_n$	P_n/Ω_c	$\phi_c P_n$	P_n/Ω_c	$\phi_c P_n$	P_n/Ω_c	$\phi_c P_n$	P_n/Ω_c	$\phi_c P_n$	P_n/Ω_c	$\phi_c P_n$	P_n/Ω_c	$\phi_c P_n$	P_n/Ω_c	$\phi_c P_n$							
	ASD	LRFD	ASD	LRFD	ASD	LRFD	ASD	LRFD	ASD	LRFD	ASD	LRFD	ASD	LRFD	ASD	LRFD							
Shape	WT5x	50.0	44.0	38.5	34.0	30.0	27.0	24.5															
F_y	36 ksi																						
Effective Length KL (ft)	6	123.4	185.5	114.0	171.3	103.7	155.8	94.0	141.2	86.8	130.4	80.3	120.7	74.3	111.7								
	7	116.4	174.9	107.1	161.0	97.0	145.8	87.5	131.6	80.6	121.1	74.3	111.7	68.7	103.2								
	8	108.9	163.6	99.7	149.9	89.9	135.2	80.9	121.6	74.3	111.6	68.2	102.5	62.9	94.6								
	9	101.3	152.2	92.4	138.9	82.9	124.6	74.3	111.7	68.0	102.2	62.1	93.4	57.2	86.0								
	10	93.8	141.0	85.2	128.0	76.0	114.3	68.0	102.1	61.9	93.1	56.3	84.7	51.8	77.8								
	11	86.5	130.0	78.2	117.6	69.5	104.4	61.9	93.0	56.2	84.4	50.9	76.5	46.7	70.2								
	12	79.5	119.5	71.6	107.6	63.2	95.0	56.1	84.3	50.8	76.3	45.8	68.8	41.9	63.0								
	13	72.9	109.5	65.3	98.2	57.4	86.3	50.8	76.3	45.8	68.8	41.1	61.7	37.5	56.4								
	14	66.6	100.1	59.5	89.4	51.9	78.1	45.8	68.8	41.1	61.8	36.8	55.3	33.5	50.4								
	15	60.7	91.2	54.0	81.2	47.0	70.6	41.3	62.1	37.1	55.7	33.1	49.7	30.1	45.3								
	16	55.4	83.3	49.2	74.0	42.7	64.2	37.5	56.4	33.6	50.5	29.9	44.9	27.2	40.9								
	17	50.8	76.4	45.0	67.6	39.0	58.6	34.2	51.4	30.5	45.9	27.1	40.8	24.7	37.1								
Effective Length KL (ft)	18	46.7	70.2	41.3	62.1	35.7	53.6	31.3	47.0	27.9	41.9	24.7	37.2	22.5	33.8								
	19	43.1	64.8	38.0	57.2	32.8	49.3	28.7	43.1	25.6	38.4	22.6	34.0	20.6	30.9								
	20	39.9	59.9	35.1	52.8	30.2	45.4	26.4	39.7	23.5	35.3												
	21	37.0	55.6	32.5	48.9																		
	22																						
F_y	50 ksi	50.0	44.0	38.5	34.0	30.0	27.0	24.5															
Effective Length KL (ft)	6	160.8	241.8	147.9	222.3	134.0	201.3	120.9	181.7	111.3	167.3	102.5	154.1	94.8	142.4								
	7	148.6	223.3	136.0	204.4	122.5	184.0	110.1	165.5	101.0	151.8	92.6	139.1	85.4	128.3								
	8	136.2	204.7	124.0	186.4	111.0	166.9	99.4	149.4	90.8	136.5	82.8	124.5	76.2	114.6								
	9	124.1	186.5	112.4	169.0	100.0	150.3	89.2	134.1	81.1	121.9	73.5	110.5	67.5	101.5								
	10	112.5	169.1	101.4	152.4	89.7	134.8	79.6	119.6	72.1	108.3	65.0	97.7	59.6	89.5								
	11	101.6	152.6	91.1	136.9	80.0	120.2	70.7	106.3	63.8	95.9	57.3	86.1	52.3	78.7								
	12	91.4	137.3	81.5	122.4	71.1	106.9	62.6	94.1	56.3	84.6	50.3	75.6	45.9	69.0								
	13	81.8	123.0	72.7	109.3	63.3	95.1	55.6	83.6	49.9	74.9	44.4	66.8	40.5	60.9								
	14	73.7	110.7	65.3	98.1	56.6	85.1	49.7	74.7	44.4	66.8	39.5	59.4	36.0	54.1								
	15	66.6	100.1	58.9	88.5	51.0	76.6	44.7	67.1	39.9	59.9	35.4	53.2	32.2	48.4								
	16	60.5	91.0	53.4	80.3	46.1	69.3	40.3	60.6	35.9	54.0	31.8	47.9	29.0	43.5								
	17	55.2	83.0	48.6	73.1	41.9	62.9	36.6	55.0	32.6	48.9	28.8	43.3	26.2	39.3								
Effective Length KL (ft)	18	50.5	76.0	44.4	66.8	38.2	57.4	33.4	50.1	29.6	44.5	26.2	39.4	23.8	35.7								
	19	46.4	69.8	40.8	61.3	35.0	52.6	30.5	45.9	27.1	40.7	23.9	35.9	21.7	32.6								
	20	42.8	64.3	37.5	56.4	32.2	48.3	28.0	42.1	24.8	37.3												
	21	39.6	59.5	34.6	52.1																		
	22																						
Properties	ASD	LRFD	^S Shape is slender for compression																				
A_g (in. ²)			14.70	13.00	11.30	10.00	8.84	7.90	7.21	$t_1 = \text{Roundup}(t_{\text{flange}} / 0.125") \times 1/8$													
γ_{\min} (in.)			1.29	1.27	1.24	1.22	1.21	1.19	1.18														
$\Omega_c = 1.67$	$\phi_c = 0.9$		Notes: Heavy lines indicates KL/r equal to or greater than 120, 140, & 200 respectively																				
			Stem of the Tee orientates horizontally																				

Available Strength in Axial Compression, Kips Eccentrically Loaded WTs

Design	P_n/Ω_c	$\phi_c P_n$	P_n/Ω_c	$\phi_c P_n$	P_n/Ω_c	$\phi_c P_n$	P_n/Ω_c	$\phi_c P_n$	P_n/Ω_c	$\phi_c P_n$	P_n/Ω_c	$\phi_c P_n$	P_n/Ω_c	$\phi_c P_n$	
	ASD	LRFD	ASD	LRFD	ASD	LRFD	ASD	LRFD	ASD	LRFD	ASD	LRFD	ASD	LRFD	
Shape	WT5x														
	22.5	19.5	16.5	15.0	13.0	11.0	9.5								
F_y	36 ksi														
Effective Length KL (ft)	6	67.3	101.2	59.6	89.6	52.6	79.1	45.6	68.6	40.4	60.8	34.4	51.8	24.4	36.7
	7	62.7	94.2	55.5	83.4	49.0	73.7	43.3	65.0	38.3	57.5	32.6	49.0	22.4	33.6
	8	57.9	87.0	51.2	77.0	45.3	68.1	40.7	61.2	36.0	54.1	30.7	46.1	20.2	30.4
	9	53.1	79.9	47.0	70.6	41.6	62.5	38.0	57.2	33.6	50.4	28.7	43.1	17.9	27.0
	10	48.5	72.9	42.8	64.4	37.9	57.0	35.4	53.2	31.2	46.8	26.6	40.0	15.7	23.6
	11	44.1	66.3	38.9	58.5	34.5	51.8	32.7	49.2	28.8	43.3	24.6	37.0	13.6	20.5
	12	40.0	60.1	35.2	52.9	31.2	46.9	30.2	45.4	26.5	39.8	22.6	34.0	11.9	17.9
	13	36.1	54.3	31.8	47.7	28.2	42.3	27.7	41.7	24.3	36.5	20.7	31.2	10.5	15.8
	14	32.5	48.9	28.6	43.0	25.4	38.1	25.4	38.2	22.2	33.4	18.9	28.4	9.3	14.0
	15	29.3	44.1	25.7	38.7	22.8	34.3	23.2	34.9	20.3	30.5	17.2	25.8		
	16	26.5	39.9	23.3	35.0	20.6	31.0	21.2	31.8	18.4	27.7	15.6	23.5		
	17	24.1	36.3	21.2	31.8	18.7	28.1	19.3	29.0	16.8	25.2	14.2	21.4		
18	22.0	33.1	19.3	29.0	17.1	25.7	17.7	26.6	15.4	23.1	13.0	19.6			
19	20.2	30.4	17.7	26.6	15.6	23.5	16.3	24.5	14.1	21.2	11.9	18.0			
20	18.6	27.9	16.3	24.4	14.4	21.6	15.0	22.6	13.0	19.6	11.0	16.5			
21					13.2	19.9	13.9	20.9	12.0	18.1	10.2	15.3			
22							12.9	19.4	11.1	16.8	9.4	14.1			
F_y	50 ksi														
Effective Length KL (ft)	6	86.5	130.0	76.6	115.2	67.7	101.8	59.4	89.2	50.3	75.6	41.1	61.7	29.5	44.3
	7	78.8	118.4	69.6	104.7	61.6	92.6	55.2	83.0	47.2	70.9	38.8	58.3	26.3	39.5
	8	71.0	106.8	62.7	94.3	55.5	83.5	51.0	76.6	43.7	65.6	36.2	54.4	23.0	34.6
	9	63.6	95.7	56.1	84.4	49.7	74.7	46.7	70.2	40.1	60.3	33.4	50.3	19.7	29.6
	10	56.7	85.2	49.9	75.1	44.3	66.5	42.5	63.9	36.6	55.0	30.7	46.1	16.8	25.3
	11	50.3	75.6	44.3	66.6	39.3	59.0	38.5	57.9	33.3	50.0	27.9	42.0	14.5	21.8
	12	44.5	66.9	39.1	58.8	34.7	52.2	34.8	52.3	30.1	45.2	25.3	38.1	12.6	18.9
	13	39.4	59.2	34.6	52.0	30.7	46.1	31.2	47.0	27.1	40.7	22.9	34.4	11.0	16.6
	14	35.1	52.8	30.8	46.3	27.3	41.0	28.0	42.1	24.3	36.5	20.5	30.8	9.7	14.6
	15	31.5	47.4	27.6	41.5	24.4	36.7	25.2	37.9	21.9	32.9	18.5	27.8		
	16	28.4	42.7	24.9	37.4	22.0	33.0	22.8	34.3	19.8	29.7	16.7	25.1		
	17	25.7	38.7	22.5	33.8	19.9	29.9	20.8	31.2	18.0	27.0	15.2	22.8		
18	23.4	35.2	20.5	30.8	18.1	27.2	19.0	28.5	16.4	24.6	13.8	20.8			
19	21.4	32.2	18.7	28.1	16.5	24.8	17.4	26.1	15.0	22.6	12.6	19.0			
20	19.6	29.5	17.1	25.8	15.1	22.7	16.0	24.0	13.8	20.7	11.6	17.4			
21					13.9	20.9	14.7	22.2	12.7	19.1	10.7	16.1			
22							13.6	20.5	11.7	17.7	9.9	14.8			
Properties															
A_g (in. ²)	6.63		5.73		4.85		4.42		3.81		3.24		2.81		
γ_{min} (in.)	1.24		1.24		1.26		1.37		1.36		1.33		0.874		
ASD	LRFD	^S Shape is slender for compression $t_1 = \text{Roundup}(t_{flange} / 0.125") \times 1/8$													
$\Omega_c = 1.67$	$\phi_c = 0.9$	Notes: Heavy lines indicates KL/r equal to or greater than 120, 140, & 200 respectively Stem of the Tee orientates horizontally													

References

- [1] AISC (2010), *Manual of Steel Construction, 14th Edition*, American Institute of Steel Construction, Inc., Chicago, Illinois.
- [2] AISC (2010a), *Specification for Structural Steel Buildings, June 2010*, American Institute of Steel Construction, Inc., Chicago, Illinois.
- [3] AISC (2011), *Design Examples, Version 14, 2011*, American Institute of Steel Construction, Inc., Chicago, Illinois.
- [4] Gordon, M. E. (2010), "Tables for Eccentrically-Loaded WT Shapes in Compression," *AISC Engineering Journal*, 2nd Quarter, 2010, pp. 91-100.
- [5] Rhodes, S. and Cakebread, T. (2013), "Understanding Buckling Behavior and Using FE in Design of Steel Bridges," *International Bridge Conference*, Pittsburg, 2013.
- [6] LUSAS Bridge Software, Version 15.2 (2016), FEA Ltd, Kingston-Upon-Thames, UK.
- [7] Galambos, T. V. (2001), "Strength of Singly Symmetric I-Shaped Beam-Columns," *AISC Engineering Journal*, 2nd Quarter, 2001, pp. 65-77.
- [8] Ellifritt, D. S., et al. (1992), "Flexural Strength of WT Sections," *AISC Engineering Journal*, 2nd Quarter, 1992, pp. 67-74.
- [9] Tito, J. A. (2013), "Eccentric Compression Test of WT Shape Steel Braces," *11th LACCEI Latin American and Caribbean Conference for Engineering and Technology*, 2013, Cancun, Mexico.
- [10] Li, Y. W. (2012), "Axial Capacities of Eccentrically Loaded Equal-Leg Single Angles: Comparisons of Various Design Methods," *AISC Engineering Journal*, 4th Quarter, 2012, pp. 131-167.